Analysis and Simulation of Single-Phase and Two-Phase Axial Flux Brushless Dc Motor

Reaza Ashrafi Habibabadi, Amir Nekoubin
Department of Electrical Engineering
Natanz Branch, Islamic Azad University
Iran
nekoubin@yahoo.com, reza_ashrafi60@yahoo.com

Abstract: –The objective of the paper is to analyze and compare the performances of the axial flux permanent magnet brushless dc (AFPM BLDC)motor with single-phase winding and two-phase winding. To study the motor operation, a mathematical dynamic model has been proposed for each of the motor with different winding, which became the basis for simulations that were performed using MATLAB/SIMULINK software package. The calculation results show that the two-phase motor version develops more smooth torque and reaches higher efficiency than the single-phase version. However the advantage of using a single-phase version is simpler and cheaper converter which the motor is supplied from. This implicates of using this type of motor for fans and pumps where torque ripple is not the subject, while the two-phase motor can be applied where more smooth torque is required. Both motors are supplied from inverter whose structure depends on the type of winding. Since there were voltage type inverters, the switching angle of transistors had significance on the motor performance. This influence was studied for both motors.

Keywords: – Brushless DC motor, Switching angle, Inverter, and Dynamic

1 Introduction

PM machines are increasingly becoming dominant machines with the cost competitiveness of high energy permanent magnets [1]-[2]. These machines offer many unique features. They are usually more efficient because of the fact that field excitation losses are eliminated resulting in significant rotor loss reduction [3]-[4]. Thus, the motor efficiency is greatly improved and higher power density is achieved. Moreover, PM motors have small magnetic thickness which results in small magnetic dimensions. As for the axial flux PM machines, they have a number of distinct advantages over radial flux machines (RFM). They can be designed to have a higher power-to-weight ratio resulting in less core material [5] Moreover, they have planar and easily adjustable airgaps. The noise and vibration levels are less than the conventional machines. Also, the direction of the main air gap flux can be varied and many discrete topologies can be derived [6]-[7]. These benefits present the AFMs with certain advantages over conventional RFMs in various applications [8]-[9]-[10]. The first work focused on PM disc machines was performed in late 70s and early 80s [11]. Disc type axial flux PM machines have found growing interests in the last decade especially in the 90s and have been increasingly used in both naval and domestic applications as an alternative to conventional radial flux machines [12]-[13]. As briefly mentioned earlier, AFMs have some distinct advantages over RFMs. First, they can be designed to have a higher power-to-weight ratio resulting in less core material and higher efficiency [14]-[15]. Secondly, they are smaller in size than their radial flux counterparts and have disc shaped rotor and stator structures. This is an important feature of axial flux machines because suitable shape and size to match the space limitation is crucial for some applications such as electric vehicle [16]-[17]. Thirdly, they have planar and adjustable airgaps, which radial flux machines do not. Moreover, the direction of the main airgap flux can be varied and many discrete topologies can be derived. For instance, while the main flux traveling axially through the air gap and stator core creates an

external-rotor-internal- stator topology, the main air gap flux traveling axially through the airgap and both axially and radially in the stator core creates a second external-rotor-internal-stator topology. These features provide the AFMs with certain advantages over conventional RFMs in some applications. [18]-[19]. A possibility to obtain a very neat axial length for the machine makes axial-flux machines very attractive into applications in which the axial length of the machine is a limiting design parameter. Such applications are, for example electrical vehicles wheel motors and elevator motors. Axial flux machines have usually been used in integrated high-torque applications [20]-[21]-[22]. AFPM motors can be designed as double sided or single sided machines, with or without armature slots, with internal or external rotors and with surface mounted or interior type permanent magnets (PMs) [23]-[24]-[25]- [26]. Comparative study on the performances of slotted and slot-less versions of permanent magnet motors was done in [27]. There, it was observed that for the same amount of torque to be produced, slot-less motors need higher mmf compared to slotted motors. Owing to the supply of such high currents, these motors get heated up very fast and need special heat sinks for dissipating the heat. This is the main advantage of using slotted motors instead of slot-less motors. In this paper the calculations were done for the particular motor which was designed as a water pump with the wet rotor.

2 Axial Flux Permanent Magnet Motor Structure

Applying several axial-flux machine configurations can be found regarding the stator(s) position with respect to the rotor(s) positions and the winding arrangements giving freedoms to select the most suitable machine structure into the considered application. The object of study in this paper is double-sided AFPM brushless machine with internal salient-pole stator and two external rotors shown in Figure. 1. It is more compact than the motor with internal rotor. The double-sided rotor with PMs is located at the two sides of the stator. The stator consists of the electromagnetic elements made of ferromagnetic cores and coils wound on them. These elements are placed axially and uniformly distributed on the stator circumference and glued together by means of synthetic resin. The stator coils can be connected in single-phase and multi-phase systems. The motor of particular winding connection exhibits its unique performance that differs it from the motors of the other connection systems.

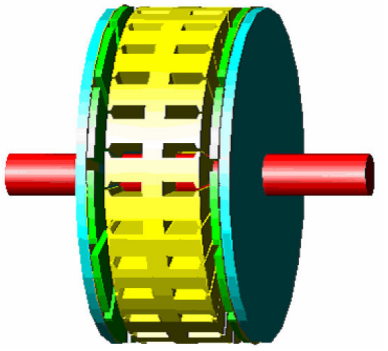

Fig. 1. Double-sided AFPM motor with two external rotors

In this paper motor with single-phase and two-phase are studied and are analyzed and compared. On both sides of the stator are the rotors made of steel discs with the permanent magnets glued to the disc surfaces. The distribution of the magnets on the rotor discs has to be adequate to the stator poles polarity. The stators winding for single-phase and two-phase motor are shown in Figure.2 and Figure.3 respectively. Here the coils of phases A and B are alternatively connected.

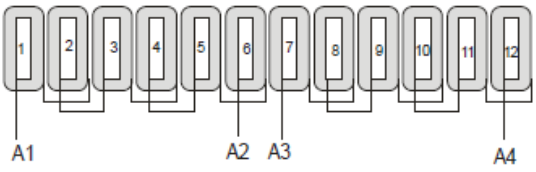

Fig .2. Windings of the stator is connected in single - phase

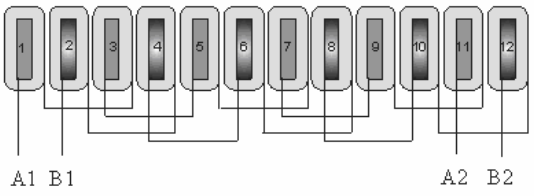

Fig .3. Windings of the stator is connected in two – phase

3 Mathematical Model of the Supply-Inverter- Motor in Single-Phase System

The supply-inverter-motor circuit model is shown in Figure.4.

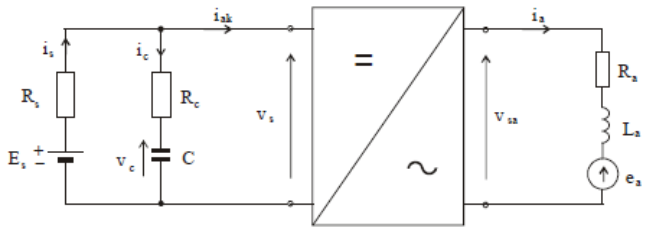

Fig. 4. Circuit diagram of supply-inverter-motor –in single-phase system

The circuit parameters are set up under the following assumptions:

• All elements of the motor are linear and no core losses are considered,

• Electromotive force ea and cogging torque vary sinusoidally with the rotational electric angle θe.

• Due to the surface mounted permanent magnets winding inductance is constant (does not change with the θe angle).

• Voltage drops across diodes and transistors and connecting wire inductance are ignored.

The equations that describe the model are as follows:

Voltage equation at the source side

$$E_s - i_s.R_s - i_c.R_c = 0 \quad (1)$$

$$V_s = V_c + i_c.R_c \quad (2)$$

$$i_s = i_{sk} + i_c \quad (3)$$

Where, Es and Rs: voltage and resistance of the source ,Rc : capacitor resistance ,is :source circuit current, iak :converter input current ,vc :voltage across capacitor

$$V_c = \frac{Q_c}{C} \quad (4)$$

Qc: charge in capacitor ,C: capacitance ,ic :current flowing through the capacitor:

$$i_c = \frac{dQ_c}{dt} \quad (5)$$

Voltage equation at the motor side:

$$La.di_a / dt + i_a R_a + e_a = v_{sa} \quad (6)$$

The voltage *sa v* that supplies the motor is a square wave and is a function of rotor position which is generated by the position sensor. So, it is described by the function.

$$sign[\sin(\theta e + \alpha)]v_s = v_{sa} \quad (7)$$

Thus the voltage equation is(8)

$$sign[\sin(\theta e + \alpha)]v_s = Ra ia + La di_a / dt + e_a \quad (8)$$

Due to the equality of the converter input and output powers (no power losses in the converter are assumed):

$$i_{ak} v_s = v_{sa}.ia \quad (9)$$

We have:

$$i_{ak} = v_{sa} / v_s.ia \quad (10)$$

The electromotive force induced in the winding

$$Ke\omega_m \sin(\theta e) = e_a \quad (11)$$

KE: constant ,ωm: rotor angular speed:

$$\omega_m = \frac{1}{P}\frac{d\theta_e}{dt} \quad (12)$$

θe: Electrical angle (Figure. 5)

p: Number of pole pairs

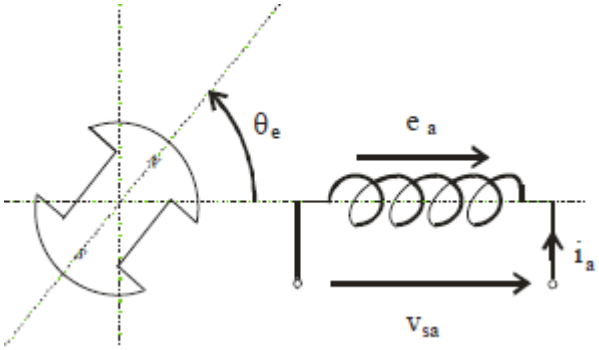

Figure.5. Calculation model of single-phase motor

The mechanical system with all torques is shown schematically in Figure. 6.

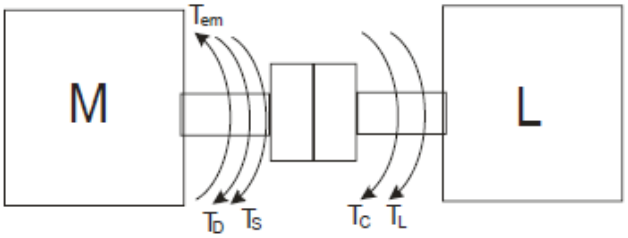

Figure .6. Mechanical system with torques

This system is defined by the following equation:

$$T_{em} = TJ + TD + Ts + Tc + TL \quad (13)$$

The torque components of equation 19 are expressed by the following equations.
Inertia torque:

$$T_J = J\frac{d\omega_m}{dt} \quad (14)$$

Viscous friction torque:

$$T_D = D.\omega_r \quad (15)$$

Coulomb friction torque:

$$Ts = sign(\omega r)Td$$

Cogging torque:

$$Tc = T_{mc}\sin(\varphi_e + \beta) \quad (16)$$

Load torque: T_L
The electromagnetic torque is given by following equation :

$$T_{em} = \frac{e_{aia}}{\omega_m} = \frac{ke\omega_m \sin\theta}{\omega_m} ia = keia\sin\theta \quad (17)$$

Other symbols used in above equations are:
J : moment of inertia, D:friction coefficient, Tmc: cogging torque amplitude, β : displacement angle of cogging torque

3.1 Simulation results of the Motor

The simulation of the motor operation in dynamic conditions was done using software package MATLAB/SIMULINK®. To simulate this operation, it was assumed that: the drive system is supplied with constant voltage of 300 V, the system is loaded with the rated torque of 6.1 N.m,. The simulation results of starting of the motor are shown in Figs 7, 8, 9, 10,11and 12. In particular the Figure.7 shows the rotary speed waveform. The ripple in the speed waveform is due to the oscillation of motor torque. It consists of two components: electromagnetic torque Tem and cogging torque Tc. These two components are shown in Figure 10, Figure 11. The results presented in Figure.11 show that the cogging torque oscillate between (-1.3, +1.3) which is not suitable. The electromagnetic torque waveform obtained during the starting process is shown in Figure 9. The results presented in Figure.12 show that the torque developed by the motor is always positive despite the relatively big cogging components. This positive resultant torque is obtained due to displacement of PMs on one of the rotor discs.

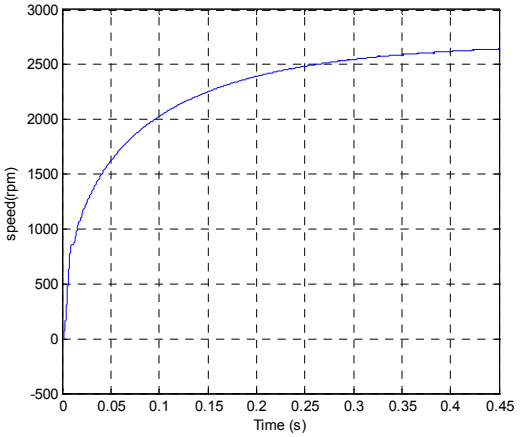

Fig.7. Waveform of rotary speed

TABLE 1. SPECIFICATIONS ADOPTED FOR THE SIMULATED MOTOR

Components	Quantity	Rating values
E b	emf of the battery	300 V
R s	source Resistance	1.5 Ω
R c	resistance in series with capacitor	2 Ω
C	capacitance	10μ F
R a	phase resistance of the brushless DC motor	8 Ω
J	moment of inertia	0.001 Kg /m2
L c	phase inductance of the brushless DC motor	0.021H
D	friction coefficient	0.001 N/(rad/s)
T load	load torque	2.2 N. m
T mc	maximum cogging torque	0.3 N.m
T s	coulomb friction torque	0.1 N.m

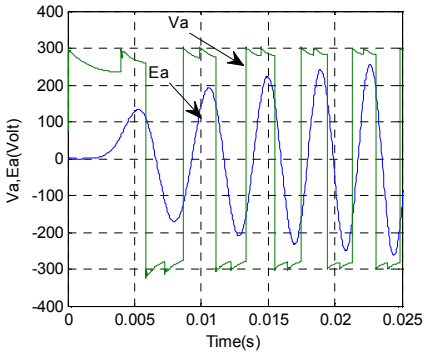

Fig .8. Waveform of EMF (Ea) and armature voltage (Va)

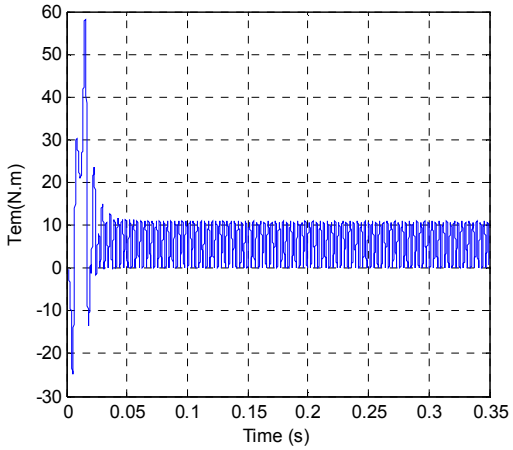

Figure. 9. Waveform of electromagnetic torque (Tem)

The waveform of EMF (Ea) and armature voltage (Va) of phase A is shown in Figs 8. The induced EMF's and voltage applied to the motor are in phase because the winding was switched ON without any delay with respect to the position of magnets and winding.

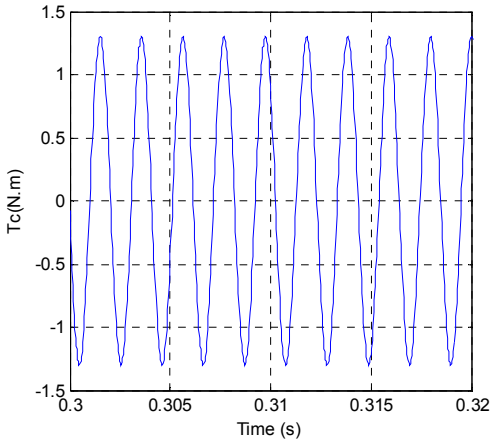

Fig .10. Waveform of cogging torque,Tc

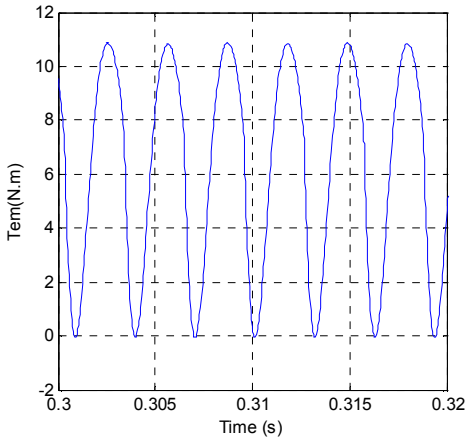

Figure .11. Waveforms of electromagnetic torque

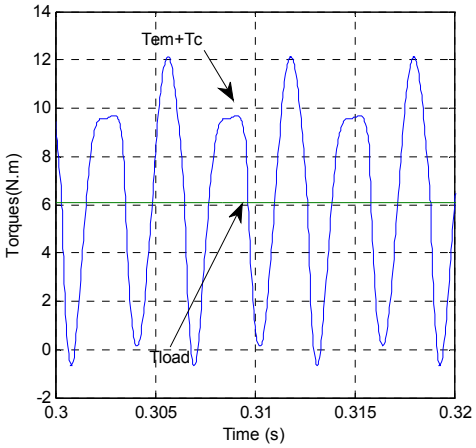

Figure .12. Waveforms of electromagnetic torque+cogging torque, load torque

4 Mathematical Model of the Supply-Inverter- Motor in Two-Phase System

The supply-inverter-motor circuit model is shown in Figure.4.

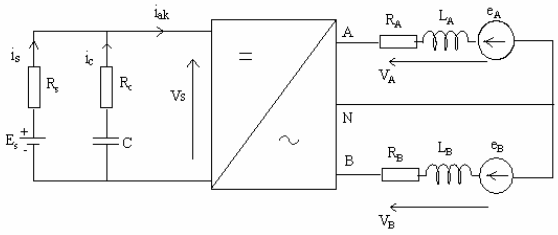

Fig. 13. Circuit diagram of supply-inverter-motor system

Voltage equations at the motor side (Figure 4) are:

$$V_A = V_{SA} \quad (18)$$

$$V_B = V_{SB} \quad (19)$$

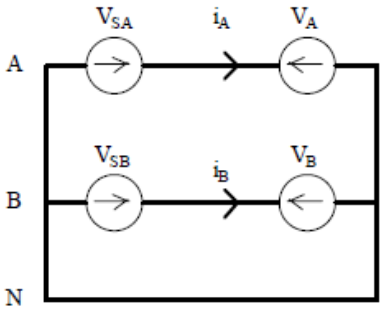

Fig.14. Scheme to the equations6,7

The equation of the voltages across the motor winding

$$\begin{bmatrix} V_A \\ V_B \end{bmatrix} = \begin{bmatrix} R_A & 0 \\ 0 & R_b \end{bmatrix} \begin{bmatrix} i_A \\ i_B \end{bmatrix} + \frac{d}{dt} \begin{bmatrix} L_A & L_{AB} \\ L_{BA} & L_B \end{bmatrix} \begin{bmatrix} i_A \\ i_B \end{bmatrix} + \begin{bmatrix} e_A \\ e_B \end{bmatrix}$$

(20)
or in shortened version:

$$V_a = R_a.I_a + \frac{d}{dt} l_a.I_a + E_a \quad (21)$$

Since the resistances Ra of all phases are the same:

$$\mathbf{R_a} = \begin{bmatrix} \mathbf{R_a} & \mathbf{0} \\ \mathbf{0} & \mathbf{R_a} \end{bmatrix} \quad (22)$$

Here there is no mutual inductance between the phases A and B, they are displaced by 90^0. So, L_{AB}, $L_{BA} = 0$. Due to the symmetrical winding the inductances $L_A = L_B = L$
The inductance matrix takes the form:

$$\mathbf{L_a} = \begin{bmatrix} \mathbf{L} & \mathbf{0} \\ \mathbf{0} & \mathbf{L} \end{bmatrix} \quad (23)$$

$$i_a + i_b = 0 \quad (24)$$

Thus the voltage equation takes the form:

$$\begin{bmatrix} \mathbf{V_A} \\ \mathbf{V_B} \end{bmatrix} = \begin{bmatrix} \mathbf{R_A} & \mathbf{0} \\ \mathbf{0} & \mathbf{R_B} \end{bmatrix} \begin{bmatrix} \mathbf{i_A} \\ \mathbf{i_B} \end{bmatrix} + \frac{\mathbf{d}}{\mathbf{dt}} \begin{bmatrix} \mathbf{L} & \mathbf{0} \\ \mathbf{0} & \mathbf{L} \end{bmatrix} \begin{bmatrix} \mathbf{i_A} \\ \mathbf{i_B} \end{bmatrix} \begin{bmatrix} \mathbf{e_A} \\ \mathbf{e_B} \end{bmatrix} \quad (25)$$

The electromotive force induced in the phase A winding:

$$\mathrm{e_a} = \mathrm{K_E}\omega_\mathrm{m}\sin(\theta_\mathrm{e}) \quad (26)$$

The electromotive force induced in the phase B winding is given by:

$$\mathrm{e_b} = \mathrm{K_E}\omega_\mathrm{m}\sin(\theta_\mathrm{e} - 90^\circ) \quad (27)$$

$$\omega_\mathrm{m} = \frac{1}{\mathrm{P}}\frac{\mathrm{d}\theta_\mathrm{e}}{\mathrm{dt}} \quad (28)$$

The electromotive forces written in a form of matrix Ea:

$$\mathbf{E_a} = \frac{\mathbf{K_E}}{\mathbf{P}} \begin{bmatrix} \mathbf{\sin\theta_e} \\ \mathbf{\sin(\theta_e - \frac{\pi}{2})} \end{bmatrix} \frac{\mathbf{d\theta_e}}{\mathbf{dt}} \quad (29)$$

Equation that links the supply and motor sides:

$$i_{SK} = \frac{1}{V_S}(i_A V_{SA} + i_B V_{SB}) \quad (30)$$

results from the equality of the powers at input and output of the inverter. Supply voltages for the phases (v_{sA}, v_{sB}) results from the operation of converter. The mechanical system is defined by the following equation 31.

$$T_{em} = T_J + T_D + T_s + T_c + T_L \quad (31)$$

The torque components of equation 19 are expressed by the following equations.
Inertia torque:

$$\mathrm{T_J} = \mathrm{J}\frac{\mathrm{d}\omega\mathrm{m}}{\mathrm{dt}} \quad (32)$$

Viscous friction torque:

$$\mathrm{T_D} = \mathrm{D}.\omega_\mathrm{r} \quad (33)$$

Coulomb friction torque:

$$Ts = sign(\omega r)Td \quad (34)$$

Cogging torque:

$$\mathrm{Tc} = \mathrm{T_{mc}}\sin(\varphi_\mathrm{e} + \beta) \quad (35)$$

Load torque: T_L

The electromagnetic torque is given by following equation 24 and 25

$$\mathrm{T_{em}} = \frac{\mathrm{e_{AiA}}}{\omega_\gamma} + \frac{\mathrm{e_{BiB}}}{\omega_\gamma} \quad (36)$$

$$\mathrm{T_{em}} = \frac{\mathrm{e_{AiA}}}{\omega_\mathrm{R}} + \frac{\mathrm{e_{BiB}}}{\omega_\mathrm{R}} = \mathrm{K_e}(\mathrm{f_a}(\theta_\mathrm{e}).\mathrm{i_A} + \mathrm{f_b}(\theta_\mathrm{e}).i_B) \quad (37)$$

Where:

$$\mathrm{f_a}(\theta_\mathrm{e}) = \sin(\theta_\mathrm{e}) \quad (38)$$

$$\mathrm{f_b}(\theta_\mathrm{e}) = \sin(\theta_\mathrm{e} - \frac{\pi}{2}) \quad (39)$$

Combining all the above equations, the system in steady-space form is:

$$\mathbf{x}\cdot = \mathbf{Ax} + \mathbf{Bu} \quad (40)$$

$$\mathbf{x} = \left[\mathbf{i_A}\ \mathbf{i_B}\ \ \omega_\gamma\ \ \theta_\mathbf{e}\right]^t \quad (41)$$

$$\mathbf{A} = \begin{bmatrix} \frac{-\mathbf{R_S}}{\mathbf{L}} & \mathbf{0} & -\frac{\mathbf{K_E}\ (\mathbf{f_a}(\theta_\mathbf{e}))}{\mathbf{L}} & \mathbf{0} \\ \mathbf{0} & \frac{-\mathbf{R}}{\mathbf{L}} & -\frac{\mathbf{K_E}(\mathbf{f_a}(\theta_\mathbf{e}))}{\mathbf{L}} & \mathbf{0} \\ \frac{\mathbf{K_E}(\mathbf{f_a}(\theta_\mathbf{e}))}{\mathbf{J}} & \frac{\mathbf{K_E}(\mathbf{f_b}(\theta_\mathbf{e}))}{\mathbf{J}} & -\frac{\mathbf{D}}{\mathbf{J}} & \mathbf{0} \\ \mathbf{0} & \mathbf{0} & \frac{\mathbf{P}}{\mathbf{2}} & \mathbf{0} \end{bmatrix}$$

$$\mathbf{B} = \begin{bmatrix} \frac{1}{L} & 0 & 0 \\ 0 & \frac{1}{L} & 0 \\ 0 & 0 & \frac{-1}{J} \\ 0 & 0 & 0 \end{bmatrix} \quad (42)$$

$$\mathbf{u} = [\mathbf{V_A} \quad \mathbf{V_B} \quad \mathbf{T_L}]^t \quad (43)$$

Equation of the motor efficiency is

$$Eff\% = \frac{P_{out}}{P_{in}}.100\% \quad (44)$$

The average input power:

$$P_{in} = \frac{1}{T}\int_0^T (V_s.i_{ak})dt \quad (45)$$

The average output power:

$$P_{out} = \frac{1}{T}\int_0^T (T_L.\omega)dt \quad (46)$$

4.1. Simulation results of the two-phase motor

The simulation results of starting of the motor are shown in Figs 15, 16, 17, 18,19, 20and 21. In particular the Figure.15 shows the rotary speed waveform. The ripple in the speed waveform is due to the oscillation of motor torque. It consists of two components: electromagnetic torque Tem and cogging torque Tc. These two components are shown in Figure 19, Figure 20. The results presented in Figure.19 show that the cogging torque oscillate between (-0.3, +0.3) which is acceptable. The electromagnetic torque waveform obtained during the starting process is shown in Figure 18. The results presented in Figure.21 show that the torque developed by the motor is always positive. This positive resultant torque is obtained due to displacement of PMs on one of the rotor discs.

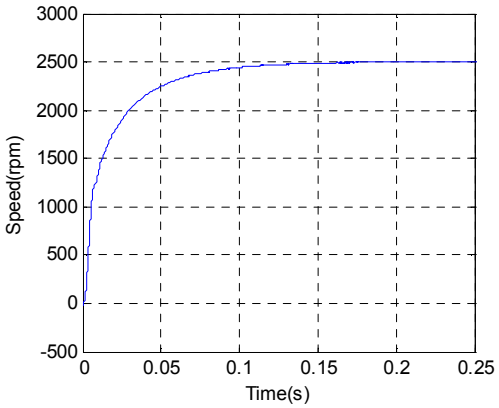

Fig. 15. Waveform of rotary speed

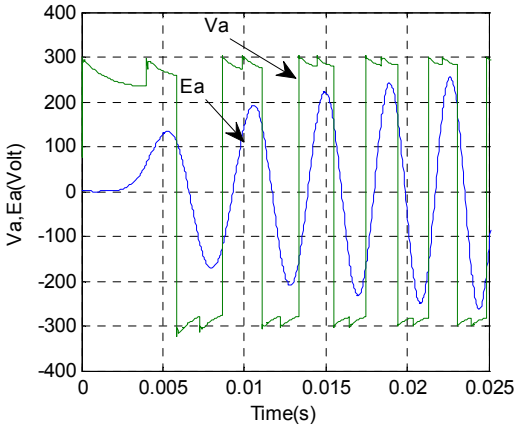

Fig .16. Waveform of EMF (Ea) and armature voltage (Va)

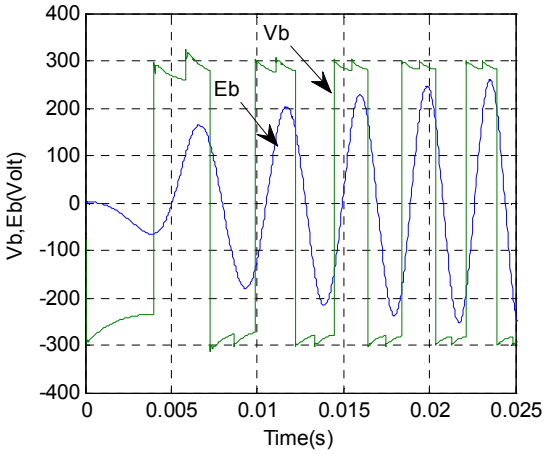

Figure. 17. Waveform of EMF (Eb) and armature voltage (Vb)

The waveform of EMF (Ea) and armature voltage (Va) of phase A and the waveform of EMF (Eb) and the armature voltage (Vb) of phase B are shown in Figs 16. and 17. The induced EMF's and voltage applied to the motor are in phase because the winding was switched ON without any delay with respect to the position of magnets and winding.

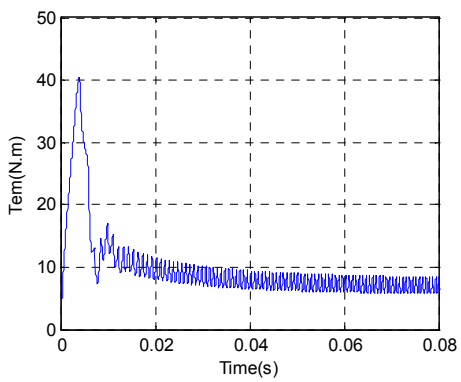

Fig .18. Waveform of electromagnetic torque (Tem)

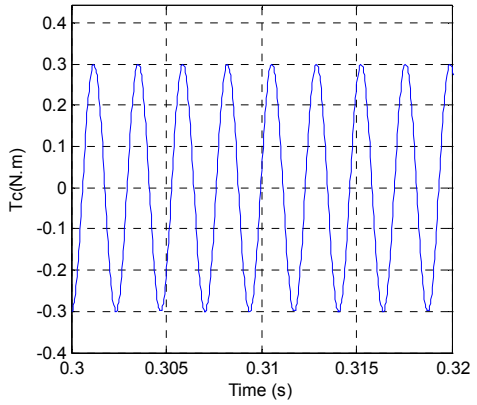

Figure .19. Waveforms of cogging torque

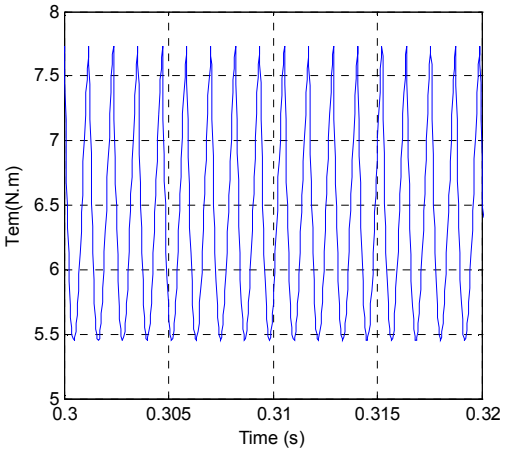

Figure .20. Waveforms of electromagnetic torque

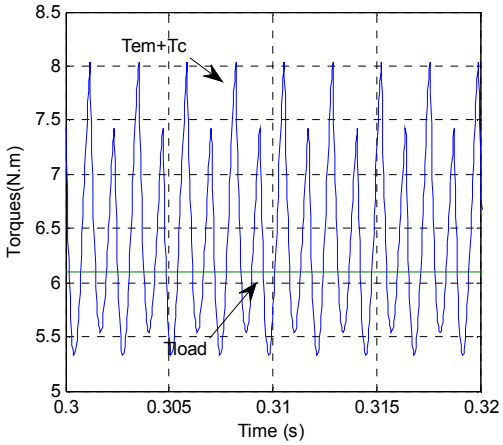

Figure .21. Waveforms of electromagnetic torque+ cogging torque , load torque

5 Influence of Switching Angle on Motors

5. 1.Single phase motor

Due to the high-speed operation, the winding inductance causes a significant phase delay in the current waveform. The results in the current and the emf waveforms being out of phase, and a negative torque component is generated, with a consequent reduction of the overall torque. In order to get motor better performance Phase commutation advanced is often employed. In DC brush motor the commutation angle is determined by the position of brushes and is kept constant. In BLDC motors the switching angle may vary accordingly to the controller of the inverter that is used. The inverter considered for the brushless motor with single-phase winding is shown in (Fig.22). The position sensors are placed between the coils in the intervals of 180 degree .These sensors sense the position of the rotor and they trigger the transistors so that they switch on the respective stator winding.

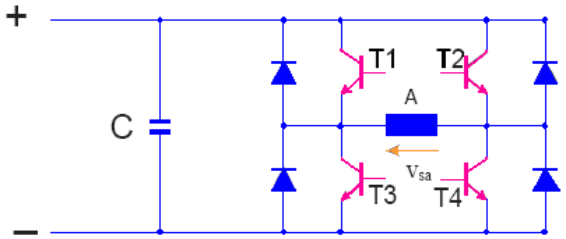

Fig. 22. Inverter considered for BLDC with single-Phase Winding

As the switching angle is advanced, the difference between back-emf and the supply voltage increases, and the torque thereby increases. However, there exists an optimal advanced angle, beyond which the drive performance deteriorates. The simulation was done for the following switching angles $\beta = -10^{\circ}, -20^{\circ}, -30^{\circ}, -40^{\circ}$. The result of simulation was plotted in the form of characteristic of average value of the efficiency shown in Fig 23. The efficiency was calculated as same as section. III. The motor efficiency is maximum when the switching angle $\beta = -30^{\circ}$, which means transistors are switched much earlier and the motor efficiency is minimum when $\beta = -10^{\circ}$.

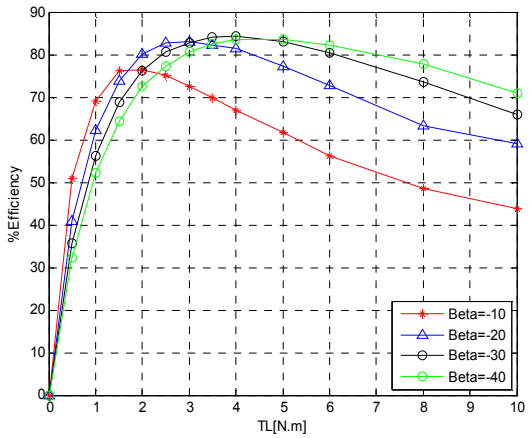

Fig. 23. Efficiency (Eff) vs. load torque(TL)

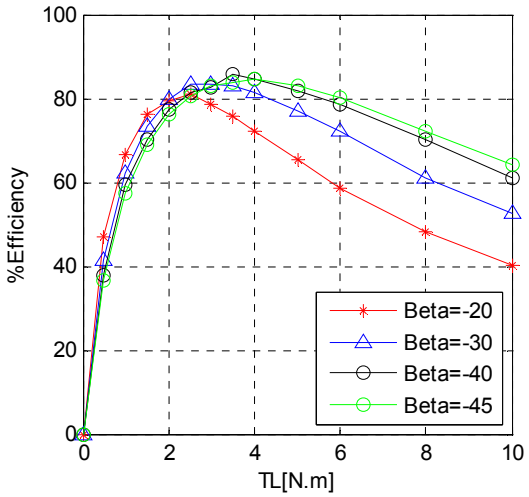

Fig. 12. Efficiency (Eff) vs. load torque(TL)

5. 2.Two-phase phase motor

The inverter considered for the brushless motor with single-phase winding is shown in (Fig.24). The position sensors are placed between the coils in the intervals of 90 degree .These sensors sense the position of the rotor and they trigger the transistors so that they switch on the respective stator winding.

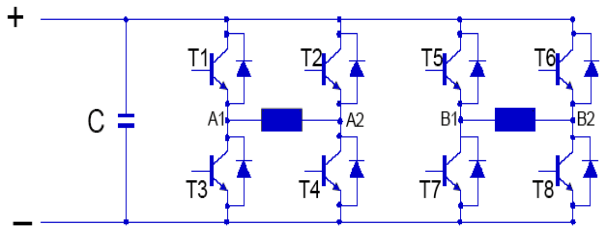

Fig. 24. Inverter considered for BLDC with Two-Phase Winding

The simulation was done for the following switching angles $\beta = -20^\circ, -30^\circ, -40^\circ, -45^\circ$. The result of simulation was plotted in the form of characteristic of average value of the efficiency shown in Fig 25. The motor efficiency is maximum when the switching angle $\beta = -40^\circ$, which means transistors are switched much earlier and the motor efficiency is minimum when $\beta = -20^\circ$.

6 Conclusion

The results obtained from dynamic model model enabled to compare both types of motors and deduct the following conclusions.

• In single-phase motor the cogging torque is very high and it contributes to an

Increase of the torque ripple. It makes the motor inapplicable where smooth torque is required. However it can be used in the drives which do not demand

Smooth torque like pumps, fans, etc.

•The two-phase motor develops the torque with lower ripple but still it cannot be applied where this cannot be tolerated e.g. wheelchair

• The advantage of the single-phase motor is the simpler commutator, which needs only one position sensor and four transistors; whereas in two-phase motor two sensors and 8 transistors are necessary which makes the circuit more complex.

• The results of simulation at rated torque show the AFPM motor with two-phase winding has higher efficiency than the AFPM motor with single-phase winding. A study done on the influence of switching angle on motor performance shows that motors operate better when the windings are switched ON earlier with respect to the emfs induced in them.

Acknowledgements
This work was supported by Natanz Branch, Islamic Azad University, IRAN.

References:

[1] Tounsi, S.; Ben Hadj, N.; Neji, R.; Sellami, F.:" Optimization of electric motor design parameters maximizing the autonomy of electric vehicles", International Review of Electrical Engineering (IREE), Vol. 2 , issue 1, JAN-FEB 2007, pp. 118-126.

[2] Camara, M. B.; Gualous, H.; Gustin, F.; Berthon, A.:"Experimental study of Buck-Boost converters with polynomial control strategy for hybrid vehicles applications", International Review of Electrical Engineering (IREE), Vol. 2, issue 4, JUL-AUG 2007,pp. 601-611.

[3] Perez-Pinal, F. J.; Nunez, C.; Alvarez, R.; Gallegos, M.:"Step by Step Design of the Power Stage of a Light Electric Vehicle", International Review of Electrical Engineering (IREE), Vol. 3, issue 1, JAN-FEB 2008, pp. 100-109.

[4] Naderi, P.; Mirsalim, M.; Bathaee, S. M. T.: "Driving/Regeneration and Stability Enhancement for a Two-Wheel-Drive Electric Vehicle", International Review of Electrical Engineering (IREE), Vol. 4 issue 1, JAN-FEB 2009,pp. 57-65.

[5] S. Meo, F. Esposito, The "EVALUATOR" Suite for the Computer-aided Analysis of Advanced Automotive Electrical Power System, International Review of Electrical Engineering (IREE), Vol. 2, n. 6, pp. 751-762, 2007.

[6] F. Esposito, V. Isastia, S. Meo: Overview on Automotive Energy Storage Systems, International Review of Electrical Engineering (IREE), vol. 4 n. 6, Nov-Dec. 2009, pp. 1122-1144.

[7] F. Esposito, G. Gentile, V. Isastia, S. Meo." A New Bidirectional Soft-Switching Multi-Input DC-DC Converter for Automotive Applications", International Review of Electrical Engineering (IREE), vol. 5 n. 4, July-August 2010, pp. 1336-1346.

[8] F. Esposito, V. Isastia, S. Meo." PSO Based Energy Management Strategy for Pure Electric Vehicles with Dual Energy Storage Systems", International Review of Electrical Engineering (IREE), vol. 5 n. 5, Sept.-October 2010, pp. 1862-1871.

[9] shak, D. Manap, N.A.A. Ahmad, M.S. Arshad, M.R., Electrically actuated thrusters for autonomous underwater vehicle, *Advanced Motion Control, 11th IEEE International Workshop, Vol. 32, pp. 619- 624, 21-24March2010.*

[10] Jong Hyun Choi, Jung Hoon Kim, Dong Ho Kim, Design and Parametric Analysis of Axial Flux PM Motors with Minimized Cogging Torque, *IEEE Transactions on Magnetics, Vol. 45, pp. 2855 - 2858 19 May. 2009.*

[11] Guoping Peng, Research on energy conversion control for small-scaled brushless DC wind power system, *IEEE Transaction Control System, vol. 9 n. 4, July 2004, pp. 629–636.*

[12] Fengge Zhang, Nikolaus Neuberger, Eugen Nolle, Peter Gruenberger, Fengxiang Wang, A New Type of Induction Machine with Inner and Outer Double Rotors, *IEEE International Conference on Power Electronics and Motion Control, Vol. 1, pp. 286-289, Jan. 2004.*

[13] K. T. Chau, Y. B. Li, J. Z. Jiang and S. X. Niu, Design and control of a PM brushless hybrid generator for wind power application, *IEEE Transaction on Magnetics, Vol. 42, n. 10, pp.349−356 ,6-8 September 2006.*

[14] D. Zhang, K.T. Chau, S. Niu and J.Z. Jiang, Design and analysis of a double-stator cup-rotor PM integrated-starter-generator*, IEEE IASAnnual Meeting, pp. 20-26, Feb. 2006.*

[15] Y. Zhang, K. T. Chau, J. Z. Jiang and D. Zhang, A finite element analytical method for electromagnetic field analysis of electric machines with free rotation, *IEEE Transaction on Magnetics, Vol. 42 n. 10, January 2006, pp. 303−309.*

[16] J. Luo, S. Huang, S. Chen, and T. A. Lipo, "Design and experiments of a novel axial flux circumferential current permanent magnet (AFCC) machine with radial airgap," in *Conf. Rec. IEEE-IAS Annu. Meeting*, vol.2, Chicago, IL, 2001, pp. 1989–1996.

[17] Jang, S.-M., H.-W. Cho, and S.-K. Choi," Design and analysis of at high speed brushless DC motor for centrifugal compressor," *IEEE Transactions on Magnetics, Vol. 43, No. 6, 2573-2575*, *June* 2007.

[18] Rabinovici, R., Magnetic field analysis of permanent magnet motors," *IEEE Transactions on Magnetic*, *Vol. 32, No. 1, 265-269, January 1996.*

[19] Qiu, Z.-J., J.-D. Xu, G. Wei, and X.-Y. Hou, "An improved time domain finite element-boundary integral scheme forelectromagnetic scattering from 3-D objects," *Progress*

InElectromagnetics Research, *PIER 75, 119-135, 2007.*

[20] C. Depollier,"The three exact components of the magnetic field createdby a radially magnetized tile permanent magnet," *Progress In Electromagnetics Research, PIER 88, 307-*319, 2008.

[21] K. Atallah and D. Howe, "A novel high performance magnetic gear,*" IEEE Trans. on Magnetics, Vol. 37, No. 4, pp. 2844−2846, 2001*.

[22] R. Datta and V.T. Ranganathan, "A method of tracking the peak power points for a variable speed wind energy conversion system," *IEEE Trans. on Energy Conversion, Vol. 18, No. 1, pp. 163−168, 2003.*

[23] Z. Q. Zhu and D. Howe," Influence of design parameters on cogging torque in permanent magnet machines, "*IEEE Trans. on Energy Conversion, Vol. 15, No. 4, pp. 407−412, 2000.*

[24] Wang Fengxiang; Wang Jiqiang, Kong Zhiguo, Zhang Fengge," Radial and Axial Force Calculation of BLDC Motor with Passive Magnetic Bearing, *Proceedings of ICIEA* 2007 pp.618-621. 23-25 May 2007.

[25] Jafarboland. M; Nekoubin, A.:" Finite-Element Analysis of Permanent Magnets Structure and Switching Angle Effects on the Efficiency of two-phase Brushless DC Motor", International Review of *Electrical Engineering (IREE), Vol. 5 , n. 5, SEP-OCT 2010, pp. 2013-2021.*

[26] M. Jafarboland, A. A. Nekoubin.:" Design and Optimization of a Double-Sided Linear Induction Based on Finite Element Method", *International Review of Electrical Engineering (IREE), Vol. 5 n. 3, JAN-FEB 2010, pp. 961-969.*

[27] Fengge Zhang, Guangwei Liu, Yongshan Shen, "Characteristic Study on a Novel PMSM with Opposite-rotation Dual Rotors," *Proceeding of International Conference on Electrical Machines and Systems, vol. 50, no. 5, pp. 920–935 8-11 Oct. 2007.*